Extended Networks of Co^{2+} and Mn^{2+} Bridged by NCS^-/N_3^- Anions and Flexible Long Spacers: Syntheses, Structures, and Magnetic Properties

Xin-Yi Wang,[a] Bao-Long Li,*[b] Xia Zhu,[b] and Song Gao*[a]

Keywords: Thiocyanate / Azide / Cobalt / Manganese / 1,2-Bis(imidazol-1-yl)ethane / 1,2-Bis(1,2,4-triazol-1-yl)ethane / Magnetic properties

Four new metal-organic polymers with SCN^-/N_3^- anion bridges and flexible long spacers L {L = bim [1,2-bis(imidazol-1-yl)ethane] and bte [1,2-bis(1,2,4-triazol-1-yl)ethane]}, $[Co(SCN)_2(bim)]$ (**1-Co**), $[Co(SCN)_2(bte)]$ (**2-Co**), $[Mn(N_3)_2(bte)]$ (**3-Mn**), and $[Mn(N_3)_2(bim)]$ (**4-Mn**), were synthesized and characterized by single-crystal X-ray diffraction studies and their magnetic properties were investigated. Complex **1-Co** is a triple-bridging chain complex with double end-to-end SCN^- anions and single *gauche*-bim spacers as bridges. Complexes **2-Co** and **3-Mn** both contain 1D chains bridged by double end-to-end SCN^- or N_3^- anions and these chains are further extended to 2D (4,4) layers by the *anti*-bte spacers. Complex **4-Mn** has a topological 3D diamond structure constructed through 1D double end-on azide-bridged Mn^{II} chains and extended through the *anti*-bim spacers. Magnetic measurements reveal that **1-Co** and **3-Mn** remain paramagnetic; the dominant magnetic coupling between Co^{II} is weak ferromagnetic and that between Mn^{II} is strong antiferromagnetic. As for **2-Co** and **4-Mn**, they show metamagnetic behavior below T_N = 2.9 and 3.0 K, respectively. Our results show that a combination of the short anion bridges (SCN^-/N_3^-) and flexible bidentate long spacers can be used to construct coordination polymers with novel topologies and interesting magnetic properties.

Introduction

In the attractive field of supermolecular chemistry and crystal engineering, long bidentate spacers provide a useful approach to new functional materials with a variety of multi-dimensional arrays and networks.[1] Because of the large separation and the inefficiency to transmit magnetic interactions, these long spacers were seldomly used to construct molecule-based magnetic materials with high magnetic-ordering temperatures. However, their abilities to form new architectures with novel topologies and interesting magnetic properties still attracts intensive attention, such as compounds constructed by rigid *N*,*N*′-bidentate spacers like 4,4′-bipyridine (4,4′-bpy), (*E*)-1,2-bis(4-pyridinyl)ethene, pyrazine, and other related ligands.[2–4] Very recently, we reported a series of compounds $M(CHOO)_2(4,4'\text{-bpy})\cdot nH_2O$ (M = Mn, Co, n = 0; M = Co, Ni, n = 5) with all 3D structures and magnetically long-range ordering.[2d] As with its azide analog $M(N_3)_2(4,4'\text{-bpy})$ (M = Mn, Fe),[2a–2c] the bidentate long spacer 4,4′-bpy efficiently tuned the topologies of these compounds and led to weak ferromagnetism.

The design of coordination polymers is highly influenced by several factors such as the coordination geometry of the central atom, the structural characteristics of the ligand molecule, the solvent system and the counterion. When rigid bifunctional ligands are used as spacers to connect metal centers, the topology of the network is usually determined by the coordination geometry of the central metal preference. Contrary to rigid ligands, the flexible ligands with conformational flexibility induce a variety of structures and may lead to the formation of the supramolecular isomers.[3i,3j] Some coordination polymers with flexible ligands have been investigated.[3,4] For example two remarkable polyrotaxane-like polymers based on 1,4-bis(imidazol-1-ylmethyl)benzene (bix) were synthesized by Robson and coworkers.[3k,3l] The flexible ligands 1,2-bis(imidazol-1-yl)ethane (bim) and 1,2-bis(1,2,4-triazol-1-yl)ethane (bte) can adopt either *gauche* (angular) or *anti* (linear) conformations (Scheme 1).[4a] We previously reported several coordination polymers in which the ligands also exhibit either *gauche* or *anti* conformations.[4] Complex $[Mn(\textit{gauche}\text{-bte})_2(NCS)_2]_n\cdot[Mn(\textit{anti}\text{-bte})(H_2O)_2(NCS)_2]_n$ contains both a double-stranded chain and a single chain in the same crystal and both *gauche* and *anti* conformations of the bte spacer.[4c]

[a] State Key Laboratory of Rare Earth Materials Chemistry and Applications & PKU-HKU Joint Laboratory on Rare Earth Materials and Bioinorganic Chemistry, College of Chemistry and Molecular Engineering, Peking University,
Beijing 100871, P. R.China
Fax: 86-10-62751708
E-mail: gaosong@pku.edu.cn
[b] College of Chemistry and Chemical Engineering, The Key Laboratory of Organic Synthesis of Jiangsu Province, Suzhou University,
Street Shizi No. 1, Suzhou 215006, P. R.China
Fax: 86-512-65224783
E-mail: blli1965@pub.sz.jsinfo.net
Supporting information for this article is available on the WWW under http://www.eurjic.org or from the author.

 DOI: 10.1002/ejic.200500151

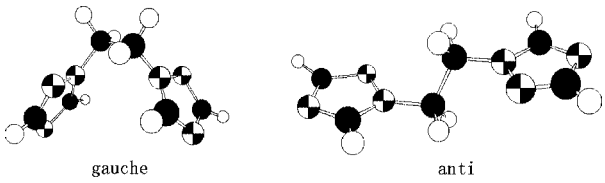

Scheme 1. The *gauche* and *anti* conformations of the bte and bim spacers (bte as example).

Of course, the main approach to constructing molecule-based magnetic materials is to employ short bridging ligands, which are efficient to mediate the magnetic coupling, to connect paramagnetic transition metal ions. Among the widely used anion ligands, the pseudohalide azide has been demonstrated to be the all-important one, if not the most, due to the versatility and the ability to mediate strong magnetic coupling, either ferro- or antiferromagnetic. Most commonly, the azide ion can adopt two possible bridging modes: end-to-end (*EE*) associated with antiferromagnetic (AF) coupling, and end-on (*EO*) related with ferromagnetic exchange.[5] In our previous reports,[2d,6] we explored another three-atom bridging ligand, the formate anion, which is a natural analog of azide, to construct new formate compounds with structures and magnetic properties similar to or different from those of azide. Furthermore, we investigated another pseudohalide anion: the thiocyanato ion (SCN^-). Like azide and formate, SCN^- can also mediate magnetic coupling between the metal ions, with the sign and the magnitude depending on the bridging modes and the localized structural details.[7–14] Owing to the two different donor groups (N and S) within it, the thiocyanate ion has less versatility and is less efficient as a magnetic coupler than the azide ligand. In contrast with the large number of azide-bridged compounds studied from a magnetic and structural point of view, there are fewer reports on the divalent first-row transition metal complexes bridged by SCN^-. Fully studied complexes are mainly compounds of Ni^{II}[8,9] and Cu^{II},[10–12] such as dimers,[8,10] 1D chains,[9,11] and 2D layers.[12] For Mn^{II} and Co^{II} compounds, the existing results are quite rare.[13,14] The 2D compounds $M(SCN)_2(ROH)_2$ (M = Mn, Co; R = CH_3, C_2H_5, C_3H_7)[13b,14] and the proposed 1D chain compounds $M(SCN)_2$(2,2-bipyridine) (M = Mn, Co) are rare examples that have been investigated thoroughly.[13a] New thiocyanate-bridged compounds, especially of Co^{II}, are needed to be explored further.

Taking into account the above-mentioned aspects, we report here the syntheses, structures and the magnetic properties of four new coordination polymers: $Co(L)(SCN)_2$ [L = bim (**1-Co**) and bte (**2-Co**)] and $Mn(L)(N_3)_2$ [L = bte (**3-Mn**) and bim (**4-Mn**)]. All four of these polymers assemble through both the flexible-bidentate long spacers (bim/bte) and the short anion ligands (SCN^-/N_3^-) as bridges. Among them, **1-Co** is a triple-bridging 1D compound bridged by double *EE*-SCN^- ligands and single *gauche*-bim spacers. **2-Co** is a 2D metamagnet with double *EE*-SCN^- ligands and *anti*-bte spacers as bridges. **3-Mn** has a very similar structure to that of **2-Co** and behaves as a magnetic AF chain. As for **4-Mn**, the double *EO*-azides and the *anti*-bim spacers lead to a metamagnet with a distorted 3D diamondoid structure.

Results and Discussion

Crystal Structures

Single-crystal X-ray diffraction of **1-Co** reveals that it crystallizes in the orthorhombic space group $Pna2_1$ and the structure is presented in Figure 1. In **1-Co**, each Co^{II} center is octahedrally coordinated by two nitrogen atoms from two bridging bim ligands in *trans* positions, two nitrogen and two sulfur atoms from four bridging *EE*-SCN^- groups. Lengthened along the S1–Co1–S2 axis, the octahedron is of an approximate D_{4h} point group. The bond lengths are as follows: Co1–N1 2.083(2), Co1–N3 2.076(2), Co1–N5 2.127(2), Co1–N6 2.122(2), Co1–S1 2.660(2), and Co1–S2 2.635(1) Å. The bond angles of D–Co1–D (D represents N or S atoms) are in the range of 88–92°. The angles of Co1–S2–C10 and Co1A–S1A–C9 are ca. 98°, which are close to a right angle, and the angles of Co1–N5–C9 and Co1A–N6A–C10 are 160° or so. So the geometry of the $Co_2(SCN)_2$ ring is close to that of a rectangle although with poor coplanarity. The geometrical feature of $Co_2(SCN)_2$ has already been observed in other thiocyanato-containing metal complexes and it is believed to have a very important influence on the magnetic coupling between the transition metal ions, especially Ni^{II}.[7a–7c,9c] It is well demonstrated that, because of the orthogonality of the orbitals, the more rectangular the geometry, the greater the possibility of ferromagnetic coupling will be.[7a–7c]

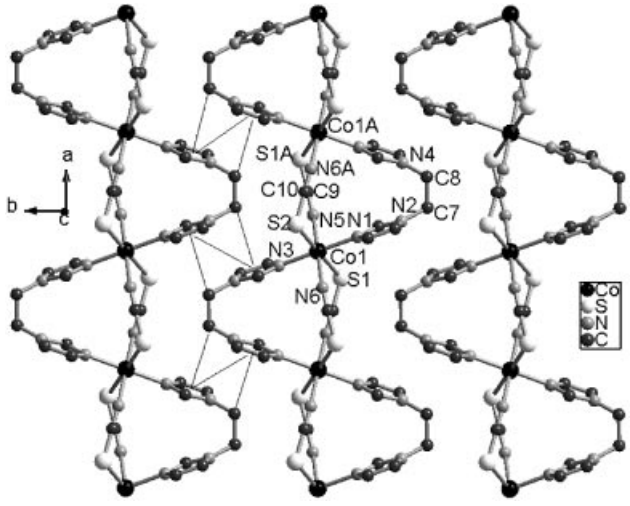

Figure 1. Toothed chain structures and the 2D layer of **1-Co**. Hydrogen atoms are omitted for clarity. The thin lines represent the π–π and C–H···π interactions between adjacent chains.

The SCN^- anion is almost linear [S1A–C9–N5 and S2–C10–N6A are 179.2(2) and 178.8(2)°, respectively] and the bim ligand is of the *gauche* conformation [torsion angle of N2–C7–C8–N4 is 59.2(3)°]. Both of these ligands act as bridges to connect adjacent Co^{II} ions to form a triple-bridg-

ing 1D toothed chain along the [100] crystallographic direction. Parallel chains stack in the [010] direction such that the convex bim bow of one chain extends into the concave section of the neighboring chain. There are obvious C–H···π interactions between the hydrogen atoms of alkanes and imidazole rings of adjacent chains (C–H···π angles 110.1 and 109.5°, and C···π distances 3.294 and 3.294 Å). Also, there are π–π interactions between the imidazole rings of the adjacent chains (perpendicular distance between centroids of the imidazole rings: 4.054 Å, dihedral angle: 0.6°). Thus, the 2D layer parallel with the *ab* plane is stabilized by these C–H···π and π–π interactions (Figure 1 and Table S1). The shortest intra- and interchain distances between Co^{II} ions are 5.625(2) and 9.095(2) Å, respectively. The layers stack together along the *c* direction in the sequence ···A–B–A–B··· with a slide of 4.55 Å (*b*/2) and the shortest Co–Co interlayer distance is about 8.170(2) Å.

Although **2-Co** has a similar composition to **1-Co** by replacing bim with bte, its structure and properties are different from **1-Co** (Figure 2). **2-Co** crystallizes in the triclinic space group $P\bar{1}$ and the Co^{II} atom is located in the symmetrical center. The cobalt atom in **2-Co** is also in the same elongated octahedron of an approximate D_{4h} point group formed by two *trans*-N atoms from bte, two *trans*-N and S atoms from four symmetry-related SCN^- anions of an *EE* mode. The bond lengths and the angles of D–Co–D are close to those of **1-Co** and the details can be found in the CIF file. Unlike **1-Co**, the ring of $Co_2(SCN)_2$ is almost coplanar and results in an approximate rectangle where the angles of Co–S–C and Co–N–C are ca. 165° and 100°, respectively, slightly larger than those in **1-Co**. Bridged by SCN^- only, **2-Co** forms 1D $[Co(SCN)_2]_n$ chains along the *a* axis; and the adjacent octahedra align parallel to one another. Different from the *gauche*-bim spacer in **1-Co**, the bte ligand in **2-Co** is of the *anti* conformation with the torsion angle N1–C3–C3A–N1A of 180.0 (2)°. Through this linear conformation, bte links adjacent cobalt chains to form a 2D neutral (4,4) network, which is very similar to that in $[Cd(NCS)_2(bte)]_n$.[4b] The 2D network in **2-Co** is completely different from the 1D toothed chain in **1-Co** only because bim in **1-Co** is replaced by bte in **2-Co**. This difference shows the subtle modulations of the bidentate spacers to construct novel topologies. The nearest Co–Co intrachain distance is 5.691(3) Å and that of the interchain is 12.014(56) Å. In the 2D network, there are no obvious π–π interactions between the adjacent triazole rings (shortest perpendicular distance between centroids of the triazole rings: 5.691 Å, dihedral angle: 0°). But, obvious π–π interactions between the 2D networks can be found (perpendicular distance between centroids of the triazole rings: 3.886 Å, dihedral angle: 0°), and there are C–H···π interactions between the hydrogen atoms of alkane and triazole rings of adjacent 2D networks (C3–H···π angles 124.5°, C···π distances 3.811 Å) (Table S2). All these weak interactions stack the 2D layers along the [011] direction in the sequence ···A–B–C–A–B–C··· to form the whole architecture (Figure S1).

The structure of **3-Mn** is very similar to that of **2-Co** (Figure 3), except that the bridging ligand is the *EE*-N_3^- anion instead of SCN^-. Also, this structure is very similar to that of $[Mn(N_3)_2(bpa)]_n$,[3m] except that the flexible bte spacer is present instead of the flexible bpa spacer. The 1D $[Mn(N_3)_2]_n$ chain is linked by bte to form a two-dimensional (4,4) layer and the layers stack along the [011] direction also in the ···A–B–C··· mode (Figure S2). There are no π–π interactions between the adjacent triazole rings in the 2D networks (shortest perpendicular distance between centroids of the triazole rings: 5.236 Å). Different from **2-Co**, the π–π interactions between adjacent 2D layers are negligibly weak (perpendicular distance between centroids of the triazole rings: 4.334 Å, dihedral angle: 0°). The coordination octahedron of Mn^{II} is more regular than that of **2-Co**; the bond lengths of Mn–N are in the range of 2.21–2.27 Å and the bond angles are from 87.0 to 93.0°. The metal–metal distance of 5.236(5) Å within the chain is shorter than that of 5.691(3) Å in **2-Co**, originating from the short length of the N_3^- ion as compared to SCN^- [2.348(8) and 2.799(10) Å for N_3^- and SCN^-, respectively]. The interchain M–M distance [11.948(56) Å] is similar to that of **2-Co** due to the same bridging ligand *anti*-bte.

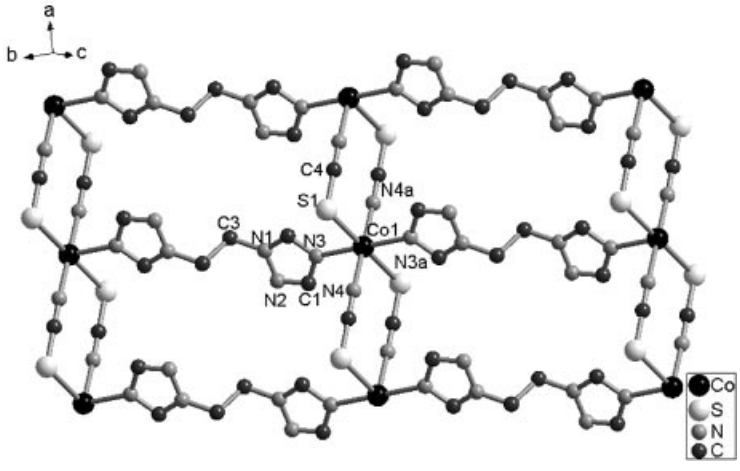

Figure 2. Two-dimensional (4,4) layer bridged by double end-to-end SCN^- and *anti*-bte ligands of **2-Co**.

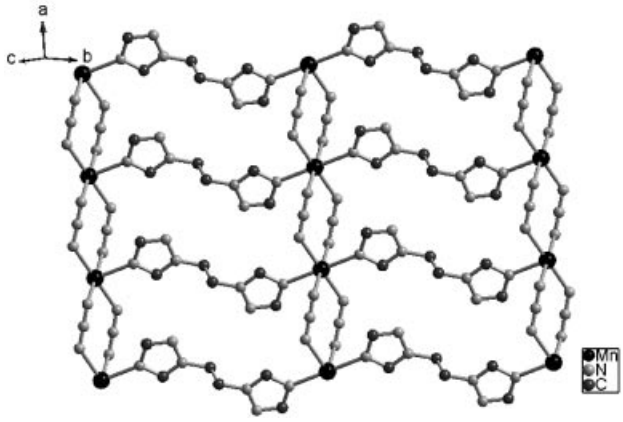

Figure 3. Two-dimensional (4,4) layer bridged by double end-to-end N_3^- and *anti*-bte ligands of **3-Mn**.

The crystal structure of **4-Mn** has some interesting characteristics. The change from the bte ligand in **3-Mn** to bim in **4-Mn** leads to very different crystal structures, which shows the importance that ancillary ligands play in tuning the crystal structure. As can be seen from Figure 4a, every Mn^{II} atom in **4-Mn** is also coordinated by six nitrogen atoms, two from the *cis*-imidazole rings of the bim ligand and the others from four *EO*-azide anions. The octahedron is largely distorted with the Mn–N bond lengths from 2.223(5) to 2.299(3) Å and N–Mn–N bond angles from 74.03(11) to 100.17(11)°. The Mn–N bond lengths do not vary much but the N–Mn–N angles deviate much from 90°, especially those of the N_{azide}–Mn–N_{azide} angles [e.g., N5–Mn1–N5a = 74.03(11)°, N8–Mn1–N8a = 77.44(11)°, and N5–Mn1–N8 = 100.17(11)°]. The detailed bond lengths and bond angles can be found in the CIF file. **4-Mn** is different from **3-Mn** in that there are two symmetrically independent azide anions (N5–N6–N7 and N8–N9–N10) and they both act as *EO* bridges, linking Mn^{II} ions to form a 1D zigzag $[Mn(N_3)_2]_n$ chain along the *a* direction (Figure 4b). The bond angles of Mn–N5–Mn and Mn–N8–Mn are 105.97(13) and 102.56(12)°, respectively, giving rise to two metal–metal intrachain distances, 3.614(5) and 3.535(5) Å, respectively. These kinds of double *EO*-azide-bridged Mn^{II} ions form a ferromagnetic chain in **4-Mn** as in two reported compounds.[2e,15]

The bim ligands in the *anti* conformation all act as bridges to expand the $[Mn(N_3)_2]_n$ chains into a 3D architecture. No obvious weak interactions can be found in **4-Mn** as the bim ligands are sufficiently separated from each other. Along the chain, the bim ligands of the Mn^{II} ions point in four different directions alternatively (Figure 4c), leading to an interesting shape of a "molecular windmill", with bim

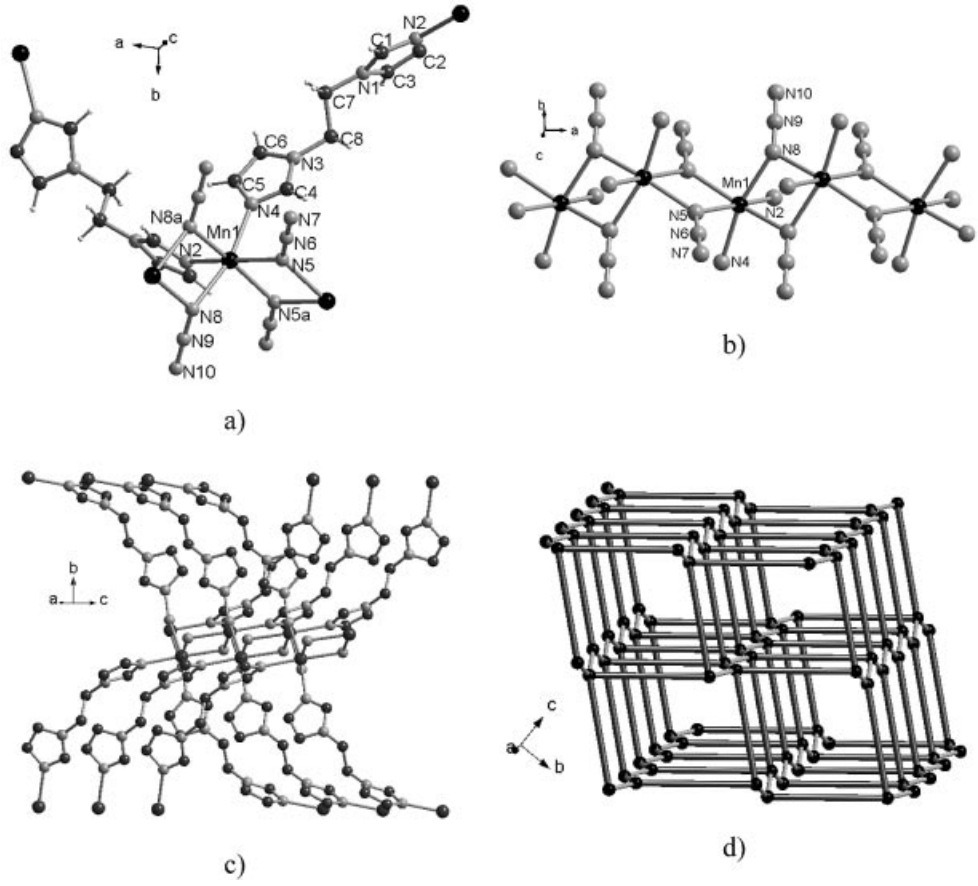

Figure 4. a) Coordination environment of Mn1 in **4-Mn**. b) Chain structure bridged by *EO*-azide anions along the *a* direction. c) Connections between adjacent chains. d) 3D distorted diamondoid topology of **4-Mn**. The long sticks represent the *anti*-bim ligands and the short ones *EO*-azide anions.

ligands in four directions as four arms. As a result of this connection mode, every Mn^{II} atom is a four-connected node, and thus the topology of **4-Mn** is a distorted 3D diamond, as can be seen in Figure 4d. If a dimer Mn^{II} bridged by azide is considered as one node, the structure can also be viewed as a simple cubic topology. The distance between the Mn^{II} ions bridged by bim is 11.460(14) Å, and such a long distance leads to porous channels along the *a* direction.

Magnetic Properties

1-Co

The plots of $\chi_M T$ versus T and χ_M^{-1} versus T measured from 2 to 300 K in 1 kOe are displayed in Figure 5. At 300 K, the $\chi_M T$ value is 3.10 $cm^3 K mol^{-1}$ and decreases to a minimum of 1.71 $cm^3 K mol^{-1}$ at 8 K, then it increases abruptly to 5.78 $cm^3 K mol^{-1}$ at 2 K. Fitting the data above 30 K using the Curie–Weiss law, $\chi_M = C/(T - \theta)$, gives a Curie constant C = 3.31 $cm^3 K mol^{-1}$, significantly larger than the spin-only value of 1.875 $cm^3 K mol^{-1}$ for Co^{2+}, and a negative Weiss constant θ of –18.8 K. Commonly, this kind of behavior of $\chi_M T$ and the negative θ value may indicate the occurrence of a dominant antiferromagnetic coupling between the spin carriers. However, because the spin-orbit coupling itself can lead to a negative θ value and a decrease of $\chi_M T$ at high temperatures, caution must be paid concerning those spins with large spin-orbit coupling, such as the Co^{2+} ion in an octahedral ligand field. Actually, the increase of $\chi_M T$ below 8 K indicates the possibility of ferromagnetic coupling. Although difficult, some efforts have been made to calculate the spin-orbit coupling parameter λ (λ = –170 cm^{-1} for the free ion), the axial splitting parameter Δ (and then the axial zero-field splitting parameter D), and/or the exchange coupling parameter J for some mono- and dinuclear Co^{II} ions in the octahedral field.[16–18] In the case of **1-Co**, we fitted the susceptibility data by considering a mononuclear Co^{2+} ion with spin-orbit coupling parameter λ ($H = -\lambda LS$) in a molecular-field approximation. The χ_{mono} for a mononuclear Co^{2+} in an octahedral environment can be calculated from Equation (1)[16] with $x = \lambda/k_B T$.

The parameter A gives a measure of the crystal field strength relative to the interelectronic repulsions and is equal to 1.5 for a weak crystal field, 1.32 for a free ion, and 1.0 for a strong field. Considering the molecular-field theory with zJ as the total exchange parameter, we can fit our experimental data above 30 K with Equation (2).[19]

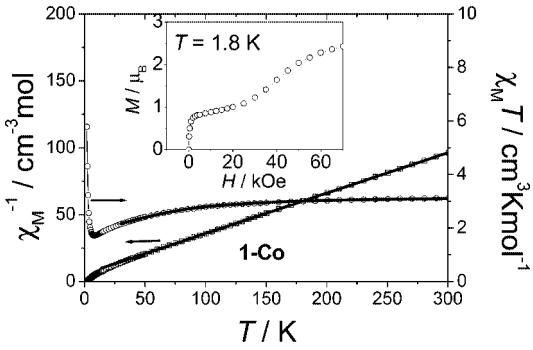

Figure 5. Plots of $\chi_M T$ versus T and χ_M^{-1} versus T from 2 to 300 K of **1-Co**. The line across χ_M^{-1} is the fit using the Curie–Weiss law and that along $\chi_M T$ represents the best fit using the model mentioned in the text. Inset: the field-dependent isothermal magnetization $M(T,H)$ for **1-Co** at 1.8 K.

$$\chi = \frac{\chi_{mono}}{1 - (2zJ/Ng^2\beta^2)\chi_{mono}} \quad (2)$$

In Equations (1) and (2), N, g, β, k_B, and T have their usual meanings. The best fit (Figure 5) gives λ = –117 cm^{-1} = –168 K, A = 1.24, and zJ = 0.42 cm^{-1} = 0.61 K with $R = 1.3 \times 10^{-5}$ [$R = \Sigma(\chi_{obsd.} - \chi_{calcd.})^2/\Sigma(\chi_{obsd.})^2$].

Although our results are semi-quantitative due to the impreciseness of the molecular-field theory, the evaluated positive zJ shows the possibility of the ferromagnetic interaction between Co^{II} neighbors. It is also evidenced by the isothermal magnetization measurement at 1.8 K (inset of Figure 5). The magnetization increases very fast from zero to about 0.7 μ_B at 2 kOe, which indicates the occurrence of ferromagnetic coupling and might suggest the occurrence of a phase transition. After a slow increase to about 1.0 μ_B at 20 kOe, the magnetization increases faster again to 2.43 μ_B at 70 kOe. To clarify the occurrence of a phase transition, the temperature dependence of the zero-field-cooled and field-cooled magnetization (ZFCM and FCM) at 20 Oe from 1.8 to 8 K, and the *ac* susceptibility under H_{dc} = 0 Oe and H_{ac} = 3 Oe from 1.8 to 4 K were measured, and the results are presented in Figure S3. All these results show no sign of long-range ordering at the lowest temperature limit of 1.8 K of our SQUID system.

2-Co

The temperature dependence of the susceptibility χ_M of **2-Co** was measured in a magnetic field of 5 kOe from 2 to 300 K and the result is plotted as $\chi_M T$ versus T and χ_M^{-1} versus T in Figure 6. After decreasing slowly upon cooling to a minimum of 3.49 $cm^3 K mol^{-1}$ at 40 K (inset of Figure 6), $\chi_M T$ increases abruptly to a peak at 4.5 K, and then

$$\chi_{mono} = \frac{1}{T} \times \frac{\frac{7(3-A)^2 x}{5} + \frac{12(2+A)^2}{25A} + \left\{\frac{2(11-2A)^2 x}{45} + \frac{176(2+A)^2}{675A}\right\} \times \exp\left(\frac{-5Ax}{2}\right) + \left\{\frac{(5+A)^2 x}{9} - \frac{20(2+A)^2}{27A}\right\} \exp(-4Ax)}{\frac{8x}{3}\left\{3 + 2\exp\left(\frac{-5Ax}{2}\right) + \exp(-4Ax)\right\}} \quad (1)$$

drops again until 2 K. The data in the range of 30–300 K obeys the Curie–Weiss law with $C = 3.79\ cm^3\,K\,mol^{-1}$ and a negative θ value of –3.50 K. As is discussed for **1-Co**, the small negative θ value does not necessarily come from the AF coupling through the *EE*-SCN^- ion but from the spin-orbit coupling. Similar to that of **1-Co**, the $\chi_M T$ data above 30 K can also be fitted by Equations (1) and (2) with a small temperature-independent paramagnetic constant $\chi_{TIP} = 0.0003\ cm^3\,mol^{-1}$. The best fit (Figure 6) gives $\lambda = -85.6\ cm^{-1} = -124$ K, $A = 1.45$ and $zJ = 2.43\ cm^{-1} = 3.51$ K with $R = 5\times10^{-6}$ [$R = \Sigma(\chi_{obsd.} - \chi_{calcd.})^2/\Sigma(\chi_{obsd.})^2$]. The A value shows the weak ligand field and the positive zJ clearly indicates the existence of the dominant ferromagnetic coupling between the adjacent Co^{II} ions, consistent with the result of **1-Co**.

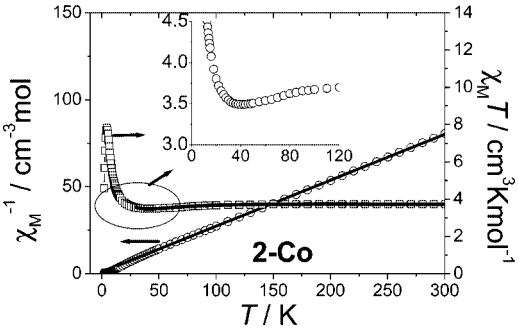

Figure 6. Plots of $\chi_M T$ versus T and χ_M^{-1} versus T from 2 to 300 K of **2-Co**.The line across χ_M^{-1} is the fit using the Curie–Weiss law and that along $\chi_M T$ represents the best fit using the model mentioned in the text. Inset: the expansion of the minimum of $\chi_M T$.

To prove the long-range ordering of **2-Co**, suggested by the peak of $\chi_M T$ at 4.5 K, we performed other measurements at low temperatures. The isothermal magnetization at 1.80 K with the field up to 50 kOe shows a pronounced sigmoid behavior of a metamagnet. The magnetization first increases slowly with increasing field strength, then shows a sharp transition to a ferromagnetic state (or a paramagnetic one) (Figure 7). At 50 kOe, the magnetization value is 2.80 μ_B, close to the expected saturated value of high-spin Co^{II}. The critical field is ca. 0.65 kOe at 1.8 K, estimated from the sharp peak of dM/dH, which is the field strength of the steepest point of the $M(H,T)$ curve. We also measured the *ac* isothermal magnetization at $H_{ac} = 3$ Oe with a dc field from –6 to + 6 kOe and a frequency of 666 Hz (Figure S4) and the FCM from 2 to 6 K at different fields (200, 400, 500, 600 and 800 Oe) (inset of Figure 7). The sharp peak of χ_M' is consistent with that of dM/dH; and the peak of χ_M in the FCM shifts to low temperatures with increasing external fields and finally disappears when the field is larger than the critical field. Also, the temperature-dependent ac susceptibility under $H_{dc} = 0$ Oe and $H_{ac} = 3$ Oe with frequencies of 277, 666, 1633, and 4111 Hz was measured from 2 to 6 K (Figure 8). The in-phase signal shows a sharp peak at ca. 2.9 K, and no detectable out-of-phase signal or frequency dependence was observed.

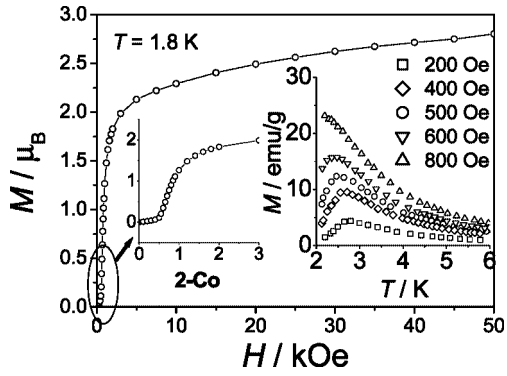

Figure 7. Field-dependent isothermal magnetization $M(T,H)$ for **2-Co** at 1.8 K. The low-field region is expanded for clarity. Inset: field-cooled magnetization from 2 to 6 K at different fields.

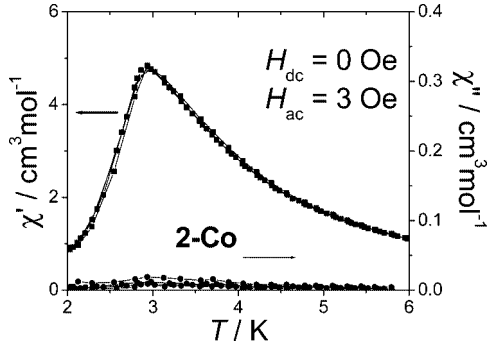

Figure 8. Ac susceptibilities from 2 to 6 K in zero applied dc field and an ac field of 3 Oe at different frequencies (277, 666, 1633, 4111 Hz) for **2-Co**.

All of the measured data indicates that **2-Co** is a metamagnet below the critical temperature 2.9 K, and the critical field for the metamagnetic transition is ca. 650 Oe at 1.8 K. Considering the structure, the metamagnetism of **2-Co** can be rationalized as a result of the competition between the weak antiferromagnetic coupling among the ferromagnetic $[Co(SCN)_2]_n$ chains and the external field. External fields larger than 650 Oe overcome the antiferromagnetic stacking of the chains and turn the AF ground state into a paramagnetic one.

3-Mn

The magnetic susceptibility χ_M of **3-Mn** measured at 10 kOe from 2 to 300 K shows a broad peak at about 50 K (Figure S5), which is typical for an AF-coupled system. As can be seen from Figure 9, the $\chi_M T$ value at 300 K is $3.61\ cm^3\,K\,mol^{-1}$, which is significantly lower than the spin-only value of $4.375\ cm^3\,K\,mol^{-1}$, and decreases continuously to $0.0387\ cm^3K\,mol^{-1}$ at 2 K. Fitting of the data above 130 K with the Curie–Weiss law gives $C = 4.94\ cm^3\,K\,mol^{-1}$ and $\theta = -108$ K, indicating a strong antiferromagnetic coupling between the Mn^{II} ions bridged by the *EE*-N_3^- anion. At 1.8 K, the isothermal magnetization $M(T,H)$ increases almost linearly from 0 to 50 kOe and reaches 0.2 μ_B per Mn^{II} atom at 50 kOe, far from the saturation value $M_S = 5\ \mu_B$ for a spin-only Mn^{II} ion, confirming the antiferromagnetic coupling between the Mn^{II} ions. Considering the

low-dimensional structure of **3-Mn**, we can fit the susceptibility data χT above 30 K using Equation (3) based on the molecular-field theory;[19] χ_{chain} is the susceptibility of the Fisher model of a 1D equally spaced Hensenberg chain for a classical spin (S = 5/2) with the Hamiltonian $H = -2J\Sigma_{<i,j>}S_i \cdot S_j$ [Equation (4)][19a] with u represented by Equation (5).

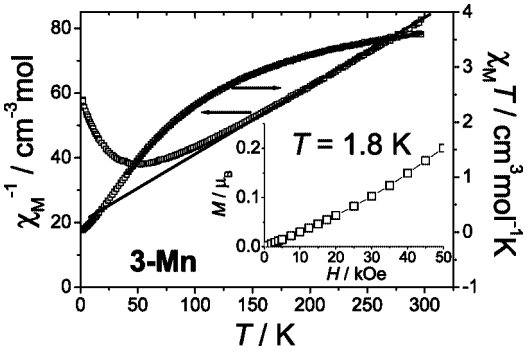

Figure 9. Plots of $\chi_M T$ versus T and χ_M^{-1} versus T from 2 to 300 K of **3-Mn**. The line across χ_M^{-1} is the fit using the Curie–Weiss law and that along $\chi_M T$ represents the best fit using the chain model mentioned in the text. Inset: field-dependent isothermal magnetization $M(T,H)$ for **3-Mn** at 1.8 K.

$$\chi = \frac{\chi_{chain}}{1 - (2zJ/Ng^2\beta^2)\chi_{chain}} \quad (3)$$

$$\chi_{chain} = \frac{Ng^2\beta^2S(S+1)}{3kT}\frac{1+u}{1-u} \quad (4)$$

$$u = \coth[\frac{JS(S+1)}{kT}] - [\frac{kT}{JS(S+1)}] \quad (5)$$

In Equations (3)–(5), S = 5/2; J and zJ represent the magnetic coupling constants of the intra- and interchains. The best fit (Figure 9) gives $J = -8.08(3)\ cm^{-1} = -11.7$ K, $zJ = -0.9(1)\ cm^{-1} = -1.3$ K, and $g = 2.057$ with $R = 4.7 \times 10^{-5}$ [$R = \Sigma(\chi_{obsd.}T - \chi_{calcd.}T)^2/\Sigma(\chi_{obsd.}T)^2$]. The negative J and zJ values show that an AF interaction exists both within and between the chains.

4-Mn

As can be seen from the plots of $\chi_M T$ versus T and χ_M^{-1} versus T measured from 2 to 300 K in 10 kOe displayed in Figure S6, the value of $\chi_M T$ increases gradually with decreasing temperature and shows a peak at 10 K. This behavior suggests intrachain ferromagnetic coupling; the decrease of $\chi_M T$ below 10 K may be due to interchain antiferromagnetic coupling or saturation effect of the field. Fitting of the data above 100 K with the Curie–Weiss law gives C = 4.16 $cm^3\,K\,mol^{-1}$ and a positive θ value of +23.5 K, also indicating the dominant ferromagnetic coupling between Mn^{II} ions transmitted by the *EO*-azide anion.

To further clarify the nature of the low-temperature phase, we have measured the FCM in different fields (200, 500, 1500 Oe) (inset of Figure 10) and the ac susceptibility under H_{dc} = 0 Oe and H_{ac} = 2 Oe from 2 to 15 K (Figure 10). The FCM at low fields of 200 and 500 Oe shows peaks at about 3.0 K but the peak disappears in the high-field region (1.5 kOe). This behavior is quite similar to that of **2-Co** and indicates a phase transition from an antiferromagnetic state to a ferromagnetic one above some critical field. Actually, the ac susceptibility under zero dc field is typical for an antiferromagnet; the in-phase signal shows a sharp peak at 3.0 K, and no detectable out-of-phase signal nor frequency dependence was observed. In order to investigate the phase transition with increasing field, the isothermal magnetization $M(T,H)$ with fields up to 70 kOe at 1.8 K (Figure 11) was measured. As a whole, the magnetization increases fast at low fields and almost reaches saturation at about 10 kOe. At the highest field of 70 kOe, the saturation value is 5.1 μ_B, very close to the saturated value of 5 μ_B for S = 5/2. Careful examination of the low-field range between 0 and 3 kOe reveals two obvious abrupt steps, with H_{c1} = 0.23 kOe and H_{c2} = 0.82 kOe, defined as the H values with the steepest slopes of the $M(H,T)$ curve (inset of Figure 11). The plateau region at 1.8 K is presumably associated with the familiar spin-flop state at the intermediate field values $H_{c1} < H < H_{c2}$. The ac isothermal magnetization under a field of H_{ac} = 2 Oe with H_{dc} from 0 to 3 kOe and a frequency of 666 Hz at 1.8 K (Figure S7) supports these two transitions. Two obvious peaks, χ'_M and χ''_M, are consistent with the peaks of dM/dH.

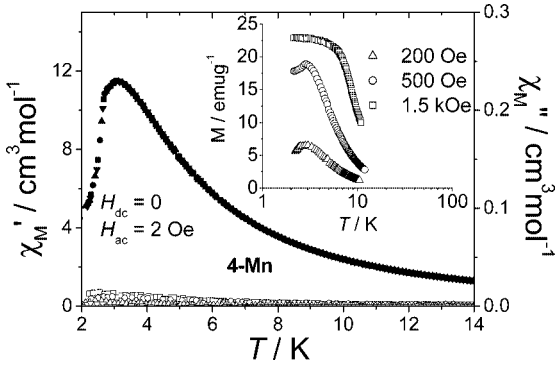

Figure 10. Ac susceptibilities from 2 to 6 K in the zero applied dc field and an ac field of 2 Oe at different frequencies (277, 666, 1633, 4111 Hz) for **4-Mn**. Inset: field-cooled magnetization at different fields.

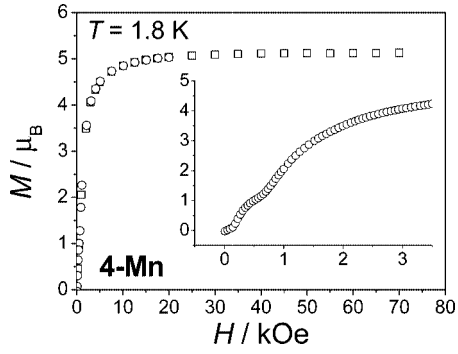

Figure 11. Field-dependent isothermal magnetization $M(T,H)$ for **4-Mn** at 1.8 K. Inset: expansion of the low-field region.

Based on the structure of **4-Mn** and the magnetic data, we rationalize that this phenomenon is a metamagnetic

transition coexisting with a spin-flop transition. The metamagnetic transition originates from competition between the external field and the AF coupling among ferro- or ferrimagnetic chains or layers. And the spin-flop transition is quite common for many antiferromagnets with weak anisotropy (for Mn^{II}, the ^6S ground state makes it one of the weakest anisotropic ions). The moment orientation switches from the easy axis to an orientation perpendicular to the applied field only when the fields are larger than a critical field H_{c1}.[19c] From the magnetic point of view, **4-Mn** can be considered as a 1D ferromagnetic chain because of the very large interchain Mn–Mn distances [11.460(14) Å] as compared to the short intrachain distances of 3.614(5) and 3.535(5) Å. The intrachain coupling transferred by the *EO*-N_3^- anion is ferromagnetic since the angles of Mn–N_{azide}–Mn are about 103° and 106°, and there are numerous reports concluding that this kind of bridging azide favors the ferromagnetic coupling between Mn^{II} ions.[2e,5a,15] With the weak AF coupling between the chains, these ferromagnetic chains are aligned in an *anti*-parallel fashion to each other at low external fields. As the field increases to a spin-flop field H_{c1} = 0.23 kOe, **4-Mn** transfers from the AF state to a spin-flop one and the antiparallel magnetizations of the two sub-lattices flop from the direction of the easy axis to that perpendicular to it. Further increase of the external field to a critical field H_{c2} = 0.82 kOe can totally overwhelm the interchain AF coupling and the state turns into a ferromagnetic one. Similar behavior was also observed in a compound where Mn^{II} and Ni^{II} ions were ferromagnetically bridged by NO_2^- anions to form a ferromagnetic chain.[20]

Conclusions

By using two flexible long ligands [1,2-bis(1,2,4-triazol-1-yl)ethane (bte) and 1,2-bis(imidazol-1-yl)ethane (bim)], and two short anion bridges SCN^- and N_3^-, we successfully synthesized four new coordination polymers formulated as $[Co(SCN)_2(bim)]$ (**1-Co**), $[Co(SCN)_2(bte)]$ (**2-Co**), $[Mn(N_3)_2(bte)]$ (**3-Mn**), and $[Mn(N_3)_2(bim)]$ **(4-Mn)**. **1-Co** crystallizes as a triple-bridging chain compound with double *EE*-SCN^- and single *gauche*-bim ligands as bridges. **2-Co** and **3-Mn** have very similar 2D (4,4) layer structures with an *anti*-bte ligand connecting $[Co(SCN)_2]_n$ or $[Mn(N_3)_2]_n$ chains bridged by double *EE*-SCN^-/N_3^- anions. **4-Mn** forms a distorted diamondoid structure through double *EO*-N_3^- and *anti*-bim bridging ligands. Magnetic measurement reveals that the dominant magnetic coupling between the Co^{II} ions in **1-Co** and **2-Co** is ferromagnetic. **1-Co** remains paramagnetic up to 1.8 K and **2-Co** is a metamagnet below T_N = 2.9 K with a critical field H_C = 650 Oe at 1.8 K. For **3-Mn**, the strong AF coupling leads to an AF chain compound without long-range ordering above 1.8 K. For **4-Mn**, the AF ground state exists below T_N = 3.0 K and a metamagnetic transition coexisting with a field-induced spin-flop transition was observed with the H_{c1} = 0.23 kOe and H_{c2} = 0.82 kOe. Our results show that a combination of short anion bridges (SCN^-/N_3^-) and flexible-bidentate long spacers can be used to construct coordination polymers with novel topologies and interesting magnetic properties.

Experimental Section

General Remarks: All starting materials were commercially available, reagent grade, and used as purchased without further purification. The ligands bim and bte were prepared according to a literature method.[21] Elemental analyses of C, H, N were carried out with a Perkin–Elmer 240C analyzer. FTIR spectra were obtained for KBr pellets with a Nicolet 170SX FTIR spectrophotometer in the 4000–400 cm^{-1} region. Variable-temperature magnetic susceptibility, zero-field ac magnetic susceptibility measurements, and field dependence of magnetization were performed with an Oxford Maglab 2000 System or a Quantum Design MPMS XL-5 SQUID system. The experimental susceptibilities were corrected for the diamagnetism of the constituent atoms (Pascal's tables).

Synthesis

$[Co(SCN)_2(bim)]$ (1-Co): $Co(NO_3)_2{\cdot}6H_2O$ (0.146 g, 0.5 mmol), KSCN (0.097 g, 1.0 mmol) and bim (0.081 g, 0.5 mmol) in 14 mL of water were heated in a Teflon-lined autoclave (20 mL) at 180 °C for 4 d. After slow cooling to room temperature, purple prism-shaped crystals suitable for single-crystal X-ray crystallographic analysis were obtained. The crystals were filtered from the mother liquor and washed with ethanol. Yield: 0.110 g (65%). $C_{10}H_{10}CoN_6S_2$ (337.29): calcd. C 35.61, H 2.99, N, 24.92; found C 35.54, H 2.96, N 24.86. IR: $\tilde{\nu}$ = 3129 (w), 2099 (vs), 1605 (w), 1520 (s), 1439 (w), 1373(w), 1285 (w), 1246 (w), 1107 (m), 1103 (m), 941 (w), 837 (w), 752 (m), 656 (m), 629 (m) and 471 (w) cm^{-1}.

$[Co(SCN)_2(bte)]$ (2-Co): $Co(NO_3)_2{\cdot}6H_2O$ (0.146 g, 0.5 mmol) and KSCN (0.097 g, 1.0 mmol) in a 20 mL solution of H_2O/EtOH (1:1, v/v) was added to one side of an H-shaped tube, and 20 mL of an H_2O/EtOH solution (1:1, v/v) of bte (0.082 g, 0.5 mmol) was added to the other side of the H-shaped tube. After approximately 3 months, purple crystals suitable for X-ray analysis were obtained. Yield: 0.090 g (53%). $C_8H_8CoN_8S_2$ (339.3): calcd. C 28.32, H 2.38, N 33.04; found C 28.24, H 2.29, N 32.86. IR: $\tilde{\nu}$ = 3121 (w), 2114 (vs), 1524 (m), 1451 (w), 1385 (m), 1319 (w), 1285 (m), 1208 (w), 1127(s), 1012 (m), 992 (m), 874 (w), 698 (w), 679 (m), 648 (m) and 463 (w) cm^{-1}.

$[Mn(N_3)_2(bte)]$ (3-Mn): A methanolic solution (20 mL) of bte (0.082 g, 0.5 mmol) was slowly added to an aqueous solution (20 mL) of $MnSO_4{\cdot}H_2O$ (0.085 g, 0.5 mmol) and excess NaN_3 (0.163 g, 2.5 mmol) while stirring. The mixtures were stirred at room temperature and the resultant solution was filtered. After the filtrate was allowed to stand in the air for 1 week, well-shaped pale yellow crystals were obtained. Yield: 0.126 g (83%). $C_6H_8MnN_{12}$ (303.1): calcd. C 23.77, H 2.66, N 55.45; found C 23.72, H 2.58, N 55.35. IR: $\tilde{\nu}$ = 3124 (w), 2076 (vs), 1780 (w), 1523 (s), 1461 (w), 1367 (w), 1281 (m), 1207 (m), 1154 (w), 1123 (m), 1010 (m), 985 (m), 893 (w), 700 (w), 679 (w), 654 (w) and 419 (w) cm^{-1}.

$[Mn(N_3)_2(bim)]$ (4-Mn): For this synthesis, $MnSO_4{\cdot}H_2O$ and bim were used in a 1:0.5 molar ratio with excess NaN_3 because the reaction of $MnSO_4{\cdot}H_2O$ and bim in a 1:1 molar ratio with excess NaN_3 will produce the complex $[Mn(N_3)_2(bim)_2]_n$.[4d] An aqueous solution (10 mL) of excess NaN_3 (0.163 g, 2.5 mmol) was mixed with 10 mL of an aqueous solution of $MnSO_4{\cdot}H_2O$ (0.170 g, 1.0 mmol) and stirred for 20 min. An ethanol solution (10 mL) of bim (0.081 g, 0.5 mmol) was then slowly added to the above solu-

Table 1. Crystallographic data for compounds **1**–**4**.

	1-Co	**2-Co**	**3-Mn**	**4-Mn**
Empirical formula	$C_{10}H_{10}CoN_6S_2$	$C_8H_8CoN_8S_2$	$C_6H_8MnN_{12}$	$C_8H_{10}MnN_{10}$
M_r [gmol^{-1}]	337.29	339.27	303.18	301.20
Crystal system	orthorhombic	triclinic	triclinic	monoclinic
Space group	$Pna2_1$	$P\bar{1}$	$P\bar{1}$	$P2_1/c$
a [Å]	11.249(3)	5.691(3)	5.236(5)	6.214(2)
b [Å]	9.095(2)	6.432(4)	6.419(6)	18.984(5)
c [Å]	12.585(3)	8.840(5)	8.760(8)	10.382(3)
α [°]	90	102.608(12)	102.752(12)	90
β [°]	90	100.220(9)	90.290(10)	89.624(5)
γ [°]	90	94.753(10)	94.551(13)	90
V [Å^3]	1287.6(6)	308.3(3)	286.2(4)	1224.6(5)
Z	4	1	1	4
$\rho_{calcd.}$ [g cm^{-3}]	1.740	1.827	1.759	1.634
Crystal size [mm^{-1}]	0.12×0.16×0.4	0.11×0.20×0.20	0.3×0.3×0.4	0.1×0.2×0.2
μ(Mo-K_α) [mm^{-1}]	1.650	1.728	1.163	1.083
Measured reflections	13604	3464	2120	11816
Independent reflections	2935	1391	1212	2166
Observed reflections[a]	2819	1264	1196	2056
No. of parameters	173	88	88	172
F(000)	684	171	153	612
GOF	1.077	1.070	0.989	1.242
Max/min [e Å^{-3}]	0.293/–0.354	0.286/–0.336	0.330/–0.237	0.227/–0.366
T_{max}/T_{min}	0.827/0.731	0.829/0.714	0.705/0.661	0.901/0.802
R_1[b]	0.0277	0.0306	0.0231	0.0535
wR_2[c]	0.0586	0.0696	0.0605	0.1169

[a] Observation criterion: $I > 2\sigma(I)$. [b] $R_1 = \Sigma||F_o| - |F_c||/\Sigma|F_o|$. $I > 2\sigma(I)$. [c] $wR_2 = \{\Sigma[w(F_o^2 - F_c^2)^2]/\Sigma[w(F_o^2)^2]\}^{1/2}$, for all data.

tion. The mixture was stirred at room temperature for 30 min and the resultant solution was filtered. After the filtrate was allowed to stand in the air for 2 weeks, well-shaped yellow crystals were obtained. Yield: 0.117 g (78%). $C_8H_{10}MnN_{10}$ (301.2): calcd. C 31.90, H 3.35, N 46.51; found C 31.79, H 3.32, N 46.38. IR: $\tilde{\nu}$ = 3125 (w), 2072 (vs), 2033 (s), 1609 (w), 1512 (m), 1466 (w), 1385 (w), 1335 (m), 1292 (w), 1261 (w), 1231 (m), 1111 (w), 1084 (s), 1022 (w), 934 (m), 830 (m), 752 (m), 664 (m) and 413 (w) cm^{-1}.

Single-Crystal X-ray Crystallography: All data collections were performed at a temperature of 193.15 K except for the crystal data collection of **2-Co** which was performed at 298(2) K with a Rigaku Mercury CCD diffractometer with ω-scan technique. The structures were solved by direct methods and refined with full-matrix least-squares techniques based on F^2 using the SHELXS-97 and SHELXL-97 programs. Anisotropic thermal parameters were assigned to all non-hydrogen atoms. The hydrogen atoms of the bte and bim ligands were generated geometrically. Details of the crystallographic data are listed in Table 1. CCDC-221765 and -260333 to -260335 contain the supplementary crystallographic data for this paper. These data can be obtained free of charge at www.ccdc.cam.ac.uk/conts/retrieving.html [or from the Cambridge Crystallographic Data Centre, 12, Union Road, Cambridge CB2 1EZ, UK; Fax: +44-1223/336-033; E-mail, deposit@ccdc.cam.ac.uk]. Also, CIF files of these four compounds can be found in the Supporting Information.

Supporting Information Available: Tables of the details of the π–π and C–H···π interactions of **1-Co** and **2-Co**, the stack of the layers of **2-Co** and **3-Mn**, ac susceptibility and ZFCM/FCM of **1-Co**, ac isothermal magnetization of **2-Co** and **4-Mn**, $\chi_M T$ versus T of **3-Mn**, $\chi_M T$ versus T, χ_M^{-1} versus T, and dM/dH of **4-Mn**.

Acknowledgments

We acknowledge support from the National Science Fund for Distinguished Young Scholars (20125104), NSFC Nos. 20221101, 20490210, and the Natural Science Foundation of the University of Jiangsu Province (No. 03KJB150118), and the Funds of The Key Laboratory of Organic Synthesis of Jiangsu Province, P. R. China. We also acknowledge Mr. Zhang Yong for the single-crystal structural determination.

[1] For examples, see: a) A. J. Blake, N. R. Champness, S. S. M. Chung, W.-Sh. Li, M. Schröder, *Chem. Commun.* **1997**, 1005–1006; b) K. N. Power, T. L. Hennigar, M. J. Zawarotko, *Chem. Commun.* **1998**, 595–596; c) C. V. K. Sharma, R. D. Rogers, *Chem. Commun.* **1999**, 83–84; d) Q.-M. Wang, G.-C. Guo, T. C. W. Mak, *Chem. Commun.* **1999**, 1849–1850; e) C. M. Grunert, J. Schweifer, P. Weinberger, W. Linert, K. Mereiter, G. Hilscher, M. Muller, G. Wiesinger, P. J. van Koningsbruggen, *Inorg. Chem.* **2004**, *43*, 155–165; f) K. Uemura, S. Kitagawa, K. Fukui, K. Saito, *J. Am. Chem. Soc.* **2004**, *126*, 3817–3828.

[2] a) S. Han, J. L. Manson, J. Kim, J. S. Miller, *Inorg. Chem.* **2000**, *39*, 4182–4185; b) S. Martín, M. G. Barandika, L. Lezama, J. L. Pizarro, Z. E. Serna, J. I. R. De Larramendi, M. I. Arriortua, T. Rojo, R. Cortés, *Inorg. Chem.* **2001**, *40*, 4109–4115; c) A.-H. Fu, X.-Y. Huang, J. Li, T. Yuen, Ch.-L. Lin, *Chem. Eur. J.* **2002**, *8*, 2239–2247; d) X.-Y. Wang, H.-Y. Wei, Z.-M. Wang, S. Gao, Zh.-D. Chen, *Inorg. Chem.* **2005**, *44*, 572–583; e) J. L. Manson, A. M. Arif, J. S. Miller, *Chem. Commun.* **1999**, 1479–1480; f) X. Hao, Y.-G. Wei, Sh.-W. Zh, *Chem. Commun.* **2000**, 2271–2272.

[3] For examples see: a) M. L. Hernández, M. G. Barandika, M. K. Urtiaga, R. Cortés, L. Lezama, M. I. Arriortua, T. Rojo, *J. Chem. Soc., Dalton Trans.* **1999**, 1401–1406; b) P. J. van Kon-

ingsbruggen, Y. Garcia, H. Kooijman, A. L. Spek, J. G. Haasnoot, O. Kahn, J. Linares, E. Codjovi, F. Varret, *J. Chem. Soc., Dalton Trans.* **2001**, 466–471; c) Y. Carcia, P. J. van Koningsbruggen, H. Kooijman, A. L. Spek, J. G. Haasnoot, O. Kahn, *Eur. J. Inorg. Chem.* **2000**, 307–314; d) S. Konar, E. Zangrando, M. G. B. Drew, T. Mallah, J. Ribas, N. R. Chaudhuri, *Inorg. Chem.* **2003**, *42*, 5966–5973; e) R. Bronisz, *Inorg. Chim. Acta* **2004**, *357*, 396–404; f) Q.-H. Zhao, H.-F. Li, X.-F. Wang, Zh.-D. Chen, *New J. Chem.* **2002**, *26*, 1709–1710; g) F. M. Tabellion, S. R. Seidel, A. M. Arif, P. J. Stang, *J. Am. Chem. Soc.* **2001**, *123*, 11982–11990; h) A. K. Ghosh, D. Ghoshal, T.-H. Lu, G. Mostafa, N. R. Chaudhuri, *Cryst. Growth Des.* **2004**, *4*, 851–857; i) T. L. Hennigar, D. C. Macquarrie, P. Losier, R. D. Rogers, M. J. Zaworotko, *Angew. Chem. Int. Ed. Engl.* **1997**, *36*, 972–973; j) B. Moulton, M. J. Zaworotko, *Chem. Rev.* **2001**, *101*, 1629–1658; k) B. F. Hoskins, R. Robson, D. A. Slizys, *J. Am. Chem. Soc.* **1997**, *119*, 2952–2953; l) B. F. Hoskins, R. Robson, D. A. Slizys, *Angew. Chem. Int. Ed. Engl.* **1997**, *36*, 2336–2338; m) M. L. Hernandez, M. G. Barandika, K. K. Urtiaga, R. Cortes, L. Lezama, M. I. Arriortua, *J. Chem. Soc., Dalton Trans.* **2000**, 79–84.

[4] a) B.-Z. Li, X. Zhu, B.-L. Li, Y. Zhang, *J. Mol. Struct.* **2004**, *691*, 159–163; b) B.-L. Li, X. Zhu, J.-H. Zhou, Y.-F. Peng, Y. Zhang, *Polyhedron* **2004**, *23*, 3133–3141; c) J.-H. Zhou, X. Zhu, Y.-N. Zhang, Y. Zhang, B.-L. Li, *Inorg. Chem. Commun.* **2004**, *7*, 949–952; d) B.-L. Li, X. Zhu, J.-H. Zhou, Y. Zhang, *Acta Crystallogr., Sect. C* **2004**, *60*, m373–m374; e) X. Zhu, B.-L. Li, J.-H. Zhou, B.-L. Li, Y. Zhang, *Acta Crystallogr., Sect. C* **2004**, *60*, m191–m193; f) L. P. Wu, Y. Yamagiwa, T. Kuroda-Sowa, T. Kamikawa, M. Munakata, *Inorg. Chim. Acta* **1997**, *256*, 155–159.

[5] For examples, see: a) J. Ribas, A. Escuer, M. Monfort, R. Vicente, R. Cortés, L. Lezama, T. Rojo, *Coord. Chem. Rev.* **1999**, *193–195*, 1027–1068; b) E.-Q. Gao, Y.-F. Yue, S.-Q. Bai, Z. He, C.-H. Yan, *J. Am. Chem. Soc.* **2004**, *126*, 1419–1429; c) T.-F. Liu, D. Fu, S. Gao, Y.-Z. Zhang, H.-L. Sun, G. Su, Y.-J. Liu, *J. Am. Chem. Soc.* **2003**, *125*, 13976–13977.

[6] X.-Y. Wang, L. Gan, S.-W. Zhang, S. Gao, *Inorg. Chem.* **2004**, *43*, 4615–4625.

[7] a) M. Kabešová, R. Boca, M. Melnícк, D. Valigura, M. Dunaj-Jurco, *Coord. Chem. Rev.* **1995**, *140*, 115–135; b) K. K. Narang, J. P. Pandey, *Synth. React. Inorg. Met.-Org. Chem.* **1994**, *24*, 73–93; c) A. H. Norbury, *Adv. Inorg. Chem. Radiochem.* **1975**, *17*, 231–386; d) R. A. Bailey, S. L. Kozak, T. W. Michelsen, W. N. Mills, *Coord. Chem. Rev.* **1971**, *6*, 407–445.

[8] a) D. M. Duggan, D. N. Hendrickson, *Inorg. Chem.* **1974**, *13*, 2929–2940; b) A. P. Ginsberg, R. L. Martin, R. W. Brookes, R. C. Sherwood, *Inorg. Chem.* **1972**, *11*, 2884–2889; c) M. Monfort, J. Ribas, X. Solans, *Inorg. Chem.* **1994**, *33*, 4271–4276; d) A. P. Ginsberg, R. C. Sherwood, R. W. Brookes, R. L. Martin, *J. Am. Chem. Soc.* **1971**, *93*, 5927–5928; e) M. Taniguchi, A. Ouchi, *Bull. Chem. Soc. Jpn.* **1986**, *59*, 3277–3278; f) J. C. Trofimenko, J. K. Calabrese, S. Wolowiec, F. B. Hulsbergen, J. Reedijk, *Inorg. Chem.* **1992**, *31*, 3943–3950; g) T. Rojo, R. Cortés, L. Lezama, M. I. Arriortus, K. Urtiga, G. Vilenueve, *J. Chem. Soc., Dalton Trans.* **1991**, 1779–1783.

[9] a) A. Escuer, S. B. Kumar, F. Mautner, R. Vicente, *Inorg. Chim. Acta* **1998**, *269*, 313–316; b) R. Vicente, A. Escuer, J. Ribas, X. Solans, *J. Chem. Soc., Dalton Trans.* **1994**, 259–262; c) B. W. Dockum, W. M. Reiff, *Inorg. Chem.* **1982**, *21*, 2613–2619.

[10] a) R. Vicente, A. Escuer, E. Peñalba, X. Solan, M. Font-Bardía, *Inorg. Chim. Acta* **1997**, *255*, 7–12; b) M. B. Cingi, A. M. Manotti Lanfredi, A. Tiripicchio, J. G. Haasnot, J. Reedijk, *Inorg. Chim. Acta* **1983**, *72*, 81–88; c) J. G. Haasnot, W. L. Driessen, J. Reedijk, *Inorg. Chem.* **1984**, *23*, 2803–2807; d) V. Kettmann, J. Krätsmár-Smogrovic, O. Svajlenová, M. Zemlicka, *Z. Naturforsch., Teil B.* **1992**, *47*, 1565–1570; e) P. C. Christidis, C. A. Bolos, G. Brauer, G. Will, N. S. Trendafilova, G. St. Nikolov, *Inorg. Chim. Acta* **1995**, *228*, 173–185.

[11] a) P. Domiano, A. Musatti, M. Nardelli, C. Peizzi, G. Predieri, *J. Chem. Soc., Dalton Trans.* **1975**, 2357–2360; b) M. Kabešová, M. Dunaj-Jurco, J. Sodánova, *Inorg. Chim. Acta* **1987**, *130*, 105–111; c) H. Yamaguchi, Y. Inomata, T. Takeuchi, *Inorg. Chim. Acta* **1990**, *172*, 105–112; d) C. A. White, G. P. A. Yap, N. P. Raju, J. E. Greedan, R. J. Crutchley, *Inorg. Chem.* **1999**, *38*, 2548–2549; e) M. Julve, M. Verdaguer, G. De Munno, J. A. Real, G. Bruno, *Inorg. Chem.* **1993**, *32*, 795–802; f) J. Ribas, C. Diaz, X. Solans, M. Font-Bardía, *J. Chem. Soc., Dalton Trans.* **1996**, 35–38; g) J. Ribas, C. Diaz, X. Solans, M. Font-Bardía, *Inorg. Chim. Acta* **1995**, *231*, 229–232; h) R. Cortés, M. K. Urtiaga, L. Lezama, J. I. R. Larramendi, M. I. Arriortua, T. Rojo, *J. Chem. Soc., Dalton Trans.* **1993**, 3685–3694; i) J. A. R. Navarro, M. A. Romero, J. M. Salas, M. Quirós, E. R. T. Tiekink, *Inorg. Chem.* **1997**, *36*, 4988–4991.

[12] S. Ferlay, G. Francese, H. W. Schmalle, S. Decurtins, *Inorg. Chim. Acta* **1999**, *286*, 108–113.

[13] a) B. W. Dockum, G. A. Eisman, E. H. Witten, W. M. Reiff, *Inorg. Chem.* **1983**, *22*, 150–156; b) G. C. Defotis, C. K. Barlowe, W. R. Shangraw, *J. Magn. Magn. Mater.* **1986**, *54–57*, 1493–1494; c) H.-J. Chen, X.-M. Chen, *Inorg. Chim. Acta* **2002**, *329*, 13–21.

[14] a) G. C. DeFotis, E. D. Remy, C. W. Scherrer, *Phys. Rev. B* **1990**, *41*, 9074–9086; b) J. N. McElearney, L. L. Balagot, *Phys. Rev. B* **1979**, *19*, 306–317; c) G. C. DeFotis, E. M. McGhee, K. R. Echols, R. S. Wiese, *J. Appl. Phys.* **1988**, *63*, 3569–3571; d) A. K. Gregson, N. T. Moxon, *Inorg. Chem.* **1982**, *21*, 586–590; e) G. C. DeFotis, B. T. Wimberly, E. M. McGhee, *J. Phys. (Paris), Colloq.* **1988**, *49*, 855–856.

[15] M. A. M. Abu-Youssef, A. Escuer, D. Gatteschi, M. A. S. Goher, F. A. Mautner, R. Vicente, *Inorg. Chem.* **1999**, *38*, 5716–5723.

[16] F. E. Mabbs, D. J. Machin, *Magnetism and Transition Metal Complexes*; Chapman and Hall, London, **1973**.

[17] B. N. Figgis, M. Gerloch, J. Lewis, F. E. Mabbs, G. A. Webb, *J. Chem. Soc. A* **1968**, 2086–2093. And references therein.

[18] H. Sakiyama, *J. Chem. Software* **2001**, *7*, 171–178. And references therein.

[19] a) O. Kahn, *Molecular Magnetism*, VCH, New York, **1993**; b) R. L. Carlin, A. J. Van-Duyneveldt, *Magnetic Properties of Transition Metal Compounds*; Springer-Verlag, New York, **1977**; c) R. L. Carlin, *Magnetochemistry*; Springer-Verlag, Berlin, Heidelberg, **1986**.

[20] R. Feyerherm, C. Mathonière, O. Kahn, *J. Phys. Condens. Matter* **2001**, *13*, 2639–2650.

[21] J. Torres, J. L. Lavandera, P. Cabildo, R. M. Claramunt, J. Elguero, *J. Heterocycl. Chem.* **1988**, *25*, 771–787.

Received: February 21, 2005
Published Online: July 14, 2005

